Enantioseparations of polyhalogenated 4,4'-bipyridines on polysaccharide-based chiral stationary phases and molecular dynamics simulations of selector-selectand interactions

Roberto Dallocchio,[1] Barbara Sechi,[1] Alessandro Dessì,[1] Bezhan Chankvetadze,[2] Sergio Cossu,[3] Victor Mamane,[4,*] Robin Weiss,[4] Patrick Pale,[4] and Paola Peluso[1,*]

[1] Istituto di Chimica Biomolecolare ICB CNR, Sede secondaria di Sassari, Sassari, Italy.

[2] School of Exact and Natural Sciences, Institute of Physical and Analytical Chemistry, Tbilisi State University, Tbilisi, Georgia.

[3] Dipartimento di Scienze Molecolari e Nanosistemi, Università Ca' Foscari Venezia, Mestre Venezia, Italy.

[4] Institut de Chimie de Strasbourg, UMR 7177, CNRS-Université de Strasbourg, Strasbourg, France.

*Correspondence should be addressed to the following authors:

Dr. Paola Peluso, Istituto di Chimica Biomolecolare, Consiglio Nazionale delle Ricerche, Traversa La Crucca 3, Li Punti, 07100 Sassari, Italy

paola.peluso@cnr.it; https://orcid.org/0000-0003-3489-3428

Dr. Victor Mamane, Institut de Chimie de Strasbourg, Centre National de la Recherche Scientifique and Université de Strasbourg, 1 rue Blaise Pascal, 67008 Strasbourg Cedex, France

vmamane@unistra.fr

Please insert ORCID for Bezhan Chankvetadze: https://orcid.org/0000-0003-2379-9815

Keywords: Bipyridines / Electrostatic potential / Enantiomer elution order / Molecular dynamics / Polysaccharide-based chiral stationary phases

Received: 23/02/2021; Revised: 12/03/2021; Accepted: 13/03/2021

This article has been accepted for publication and undergone full peer review but has not been through the copyediting, typesetting, pagination and proofreading process, which may lead to differences between this version and the Version of Record. Please cite this article as doi: 10.1002/elps.202100049.

Abbreviations: AMBER, assisted model building with energy refinement; **B3LYP**, Becke, 3-parameter, Lee-Yang-Par; **CSP**, chiral stationary phase; **DFT**, density functional theory; **EEO**, enantiomer elution order; **ESH**, explicit σ-hole; ***FR***, flow rate; **GAFF**, generalized Amber force field; **HB**, hydrogen bond; **Hex**, *n*-hexane; **IPA**, isopropanol; **MD**, molecular dynamics; **MeOH**, methanol; **MMFF**, Merck molecular force field; **MP**, mobile phase; **NP**, normal phase; **TCIBP**, 3,3',5,5'-TetraChloro-2-Iodo-4,4'-BiPyridyl; ***V***, electrostatic potential; **vdW**, van der Waals; **XB**, halogen bond

Abstract

2'-(4-Pyridyl)- and 2'-(4-hydroxyphenyl)-TCIBPs (TCIBP = 3,3',5,5'-tetrachloro-2-iodo-4,4'-bipyridyl) are chiral compounds that showed interesting inhibition activity against transthyretin fibrillation *in vitro*. We became interested in their enantioseparation since we noticed that the *M*-stereoisomer is more effective than the *P*-enantiomer. Based thereon, we recently reported the enantioseparation of 2'-substituted TCIBP derivatives with amylose-based chiral columns. Following this study, herein we describe the comparative enantioseparation of both 2'-(4-pyridyl)- and 2'-(4-hydroxyphenyl)-TCIBPs on four cellulose phenylcarbamate-based chiral columns aiming to explore the effect of the polymer backbone, as well as the nature and position of substituents on the side groups on the enantioseparability of these compounds. In the frame of this project, the impact of subtle variations of analyte and polysaccharide structures, and mobile phase (MP) polarity on retention and selectivity was evaluated. The effect of temperature on retention and selectivity was also considered, and overall thermodynamic parameters associated with the analyte adsorption onto the CSP surface were derived from van 't Hoff plots. Interesting cases of enantiomer elution order (EEO) reversal were observed. In particular, the EEO was shown to be dependent on polysaccharide backbone, the elution sequence of the two analytes being *P*-*M* and *M*-*P* on cellulose and amylose *tris*(3,5-dimethylphenylcarbamate), respectively. In this regard, a theoretical investigation based on molecular dynamics (MD) simulations was performed by using amylose and cellulose *tris*(3,5-dimethylphenylcarbamate) nonamers as virtual models of the polysaccharide-based selectors. This exploration at the molecular level shed light on the origin of the enantiodiscrimination processes.

Additional supporting information may be found in the online version of this article at the publisher's web-site.

Color online: See article online to view Figs. 1–3 and 6 in color.

Introduction

In chiral chromatography, the basic components of the recognition process are chiral analyte, chiral stationary phase (CSP), and mobile phase (MP) [1]. In this molecular environment, the chromatographic separation process originates from consecutive single adsorption and desorption steps occurring on the CSP surface as the analyte moves along the column [2,3]. Intermolecular noncovalent interactions play a pivotal role in this process, and hydrogen bonds (HBs), halogen bonds (XBs), dipole-dipole, π-π stacking, steric repulsive, and van der Waals (vdW) interactions underlie the adsorption process and the formation of transient diastereomeric assemblies between the chiral selector and the enantiomer pair [4]. The overall stereoselective contact between chiral selector and enantiomer originates from the sum of single noncovalent interactions, which is defined as steric, electrostatic or hydrophobic depending on the structural and electronic features of the interacting partners. MP polarity impacts the overall process, affecting electron density distribution and associated electrostatic potential (*V*) of the recognition sites [4,5] and, consequently, noncovalent interaction strength. A CSP represents a diffuse chirotopic environment. Indeed, as stated by Hirschmann and Hanson, chirality "*is an all-pervasive property, as it affects all parts of a chiral structure*" [6]. In the same perspective, Mislow and Siegel defined chirotopic "*any atom, and, by extension, any point or segment of the molecular model [...] that resides within a chiral environment*" [7]. On this basis, all sites of a CSP are in principle potentially able to participate in enantioselective contacts, contributing to enantiomer discrimination. This concept is particularly true for CSP with high density of chiral elements such as polysaccharide-based CSPs. Indeed, in addition to the presence of a large number of chiral centers, these polymeric CSPs are characterized by conformational chirality dependent on the helical twist generated by the specific glycosidic β- and α-1,4-linkages in cellulose and amylose chain, respectively [8]. Thus, a number of noncovalent interactions can potentially occur into the polymeric groove but, actually, only some of them act to recognize the enantiomers of a given chiral analyte, depending on its particular structure, size and shape, the sum of geometry and electronic distribution. Given this context, subtle variations of analyte and CSP structures, and MP polarity may deeply impact retention and enantioseparation on polysaccharide carbamate-based CSPs. For this reason, with the aim to detect noncovalent interactions and recognition patterns, molecular design can be fruitfully used to obtain specific structures suitable for recognition studies in liquid-phase environment. In this frame, we recently demonstrated that the structure of the 2'-substituent has a pivotal impact on the enantioseparation of 2'-substituted TCIBPs (TCIBP = 3,3',5,5'-tetrachloro-2-iodo-4,4'-bipyridyl) (Fig. 1) on amylose-based CSPs [3]. Following this study, we report herein the comparative enantioseparation of both 2'-(4-pyridyl)- (**1**) and 2'-(4-hydroxyphenyl)-TCIBPs (**2**) on four cellulose phenylcarbamate-based CSPs aiming to explore the effect of the polymer backbone, as well as the nature and position of substituents on the side groups on enantioseparability of these compounds. This issue is of interest because recently compounds **1** and **2** showed relevant inhibition activity against transthyretin fibrillation *in vitro*, the *M*-enantiomer being more effective than the *P*-enantiomer [9]. In the frame of this study, the impact of subtle variations of analyte and cellulose-based CSP structures, and MP polarity on retention and selectivity was evaluated. The effect of temperature on retention and

selectivity was also considered, and overall thermodynamic parameters associated with the analyte adsorption onto the CSP surface were derived from van 't Hoff plots. Finally, a theoretical investigation based on molecular dynamics (MD) simulations [10] was performed by using amylose and cellulose *tris*(3,5-dimethylphenylcarbamate) (A-3,5diMe and C-3,5diMe) nonamers, as virtual models of the polysaccharide-based selectors, with the aim of exploring the origin of the enantiodiscrimination processes at the molecular level.

Materials and methods

Chemicals

Compounds **1** and **2** were synthesized, purified and characterized as reported [9].

Chromatography

An Agilent Technologies (Waldbronn, Germany) 1100 Series HPLC system (high-pressure binary gradient system equipped with a diode-array detector operating at multiple wavelengths (220, 254, 280, 360 nm), and a 20 µl loop) was employed. Data acquisition and analyses were carried out with Agilent Technologies ChemStation Version B.04.03 chromatographic data software. The UV absorbance is reported as milliabsorbance units (mAU). Lux Cellulose-1 (coated) (cellulose *tris*(3,5-dimethylphenylcarbamate) (C-3,5diMe)), Lux Cellulose-2 (coated) (cellulose *tris*(3-chloro-4-methylphenylcarbamate) (C-3Cl,4Me)), Lux Cellulose-4 (coated) (cellulose *tris*(4-chloro-3-methylphenylcarbamate) (C-4Cl,3Me)), and Lux i-Cellulose-5 (immobilized) (cellulose *tris*(3,5-dichlorophenylcarbamate) (C-3,5diCl)) were used as chiral columns (5 µm, 250 ×4.6 mm) (Phenomenex Inc., Torrance, CA, USA). HPLC grade *n*-hexane (Hex), isopropanol (IPA), and methanol (MeOH) were purchased from Sigma-Aldrich (Taufkirchen, Germany). Analyses were performed in isocratic mode at 25°C. The flow rate (*FR*) was set at 0.8 ml/min. Dead time (t_0) was measured by injection of tri-*tert*butylbenzene (Sigma-Aldrich) as a non-retained compound [11]. The enantiomer elution order (EEO) was determined by injecting enantiomers of known absolute configuration [9]. The van 't Hoff experiments were conducted at 5, 10, 15, 20, 25, 30, 35, 40, and 45°C by using a thermostat jacket equipped with a RE104 LAUDA circulating water-bath (Lauda, Königshofen, Germany). When the temperature was changed, the column was allowed to equilibrate for 1 h before injecting the samples. Thermodynamic parameters were derived from the slopes and the intercepts of the van 't Hoff plots (see Supporting Information for details) by linear regression analysis. Statgraphics Centurion XVI (Statpoint Technologies, Inc., Warrenton, VA, USA) was used for all linear regression analyses.

Computationals

The 3D structures of compounds **1** and **2** and methyl 3,5-dimethylphenylcarbamate, methyl 3-chloro-4-methylphenylcarbamate, methyl 4-chloro-3-methylphenylcarbamate and methyl 3,5-dichlorophenylcarbamate, as frameworks representing the CSP side chains, were prepared using the build function, and model kits and tools provided by Spartan '10 Version 1.1.0 (Wavefunction Inc., Irvine, CA, USA) [12] for building and editing organic molecules. On this basis, molecular structures

were generated and their refinement was performed by a MMFF procedure. Then, each structure was submitted to a conformational systematic search using MMFF, spanning all shapes accessible to the molecule without regard to energy. After the elimination of duplicates and high-energy conformers, a set of energetically accessible conformers was selected. For each conformer, geometry optimization was performed employing the DFT method with the B3LYP functional and the 6-311G* basis set, and finally the respective Boltzmann distribution was constructed. Geometry optimization and computation of electrostatic potential isosurfaces (V_S) and related parameters (V_S extrema, $V_{S,max}$ and $V_{S,min}$ values, given in au) were performed by using Gaussian 09 (DFT, B3LYP, 6-311G*) (Wallingford, CT 06492, USA) [13]. Search for the exact location of such $V_{S,max}$ and $V_{S,min}$ was made through the Multiwfn code [14] and through its module enabling quantitative analyses of molecular surfaces [15]. The AMBER18 Antechamber toolkit (University of California, San Francisco, USA) [16] was used to assign the generalized Amber Force Field (GAFF) atom type and the AM1-BCC type of charge to 4,4'-bipyridines **1** and **2**. The Gaussian 09 program (DFT, B3LYP, 3-21G*) [13] was used for the *ab initio* geometry optimization calculation of the monomeric units of β-D- and α-D-glucose-1,4-dimethoxy-*tris*(3,5-dimethylphenylcarbamate). The optimized structures were used to build nonamers (9-mer) of C-3,5diMe and A-3,5diMe, respectively [17]. C-3,5diMe was characterized by a left-handed threefold (3/2) helix according to the structure reported by Vogt and Zugenmaier [18], setting the dihedral angles of the units, defined by H_1–C_1–O–$C_{4'}$(Φ) and $H_{4'}$–$C_{4'}$–O–C_1(ϕ) to 60° and 0° (Supporting Information, Fig. S1A). A-3,5diMe was characterized by a 4/3 left-handed helical structure according to the structure reported by Okamoto and co-authors [19,20], setting the dihedral angles of the units, defined by H_1–C_1–O–$C_{4'}$(Φ) and $H_{4'}$–$C_{4'}$–O–C_1(ϕ) to −68.5° and −42.0° (Fig. S1B). The terminal residues of the polymers were closed with methoxyl groups. The polymer structures were energy-minimized using the GAFF force-fields with AM1-BCC charges assigned with the Antechamber toolkit. The atoms of the backbone were fixed in their positions during the simulations by assigning a force constant of 20 kcal/mol so that, starting from the setting initial values, the applied restriction restrained the rotation of backbone dihedral angles of residues 2–8 (Fig. S2). The energies and the structure of the polymers were first prepared using 100 ns MD simulations (see Supporting Information for details about MD stages) with Hex/IPA 90:10 as medium. This structure was used in the final MD simulations. The AMBER18 software [16] was used to carry out 100 ns MD simulations. The initial positions of each enantiomer were determined by molecular docking (see Supporting Information for details). Solvent effect was taken into account by means of the explicit periodic solvent box (Hex:IPA 90:10). In this regard, the complexes polysaccharide-analyte complexes were prepared for MD runs by solvating the system with an octahedral box with a 10 Å radius polysaccharide cutoff by using Packmol-*memgen* [21,22] and an in-house script to manage solvent mixtures. 100 ns of the trajectories from each case were considered for statistical analysis. The Chimera software (UCSF, San Francisco, USA) was used for visualization and analysis of the MD trajectories [23]. Interaction energies between the polysaccharide nonamer and the enantiomer were calculated, which include vdW and electrostatic (el) energies.

Results and discussion

Electrostatic potential analysis of analytes and chiral selectors

For compounds **1** and **2**, the electrostatic potential maxima ($V_{S,max}$, Fig. 2, pale blue points) and minima ($V_{S,min}$, Fig. 2, red points) values were computed in order to inspect the electron charge density distribution on the main electron-poor (electrophile, Lewis acid) and electron-rich (nucleophile, Lewis base) recognition sites, respectively (Fig. 2A,B). Recently, *V* analysis has been fruitfully used to gain insights on selector/analyte contacts by evaluating the electron charge density on molecular regions involved in noncovalent interactions [5,24,25]. In compounds **1** and **2**, the distinctive substituents located at 2'-position are a 4-pyridyl ring in **1** and a 4-hydroxyphenyl group in **2**. Moreover, both compounds contain a common 3,3',5,5'-tetrachlorinated motif which represents a symmetric hydrophobic region surrounding the chiral axis. Another hydrophobic region is present at the 2-position where an iodine atom is located as substituent. This halogen may act as XB donor interacting through its electrophilic σ-hole with the nucleophilic regions of the CSP (Fig. 2C). Higher polarization was induced by the 4-pyridyl substituent (**1**: $V_{S,max}$ = 0.0535 au) at the position 2' of the 4,4'-bipyridinyl scaffold compared to the 4-hydroxyphenyl substituent (**2**: $V_{S,max}$ = 0.0496 au). In our previous studies, we demonstrated by chromatographic and computational analyses that the carbonyl oxygens of C-3,5diMe and A-3,5diMe are able, as Lewis bases, to form XBs with the electrophilic σ-hole regions of halogen substituents bound to the 4,4'-bipyridine rings [17]. HB sites are located on the aromatic substituents in 2'-position, a nitrogen as HB acceptor ($V_{S,min}$ = –0.0658 au) and a hydroxyl group as HB acceptor/donor ($V_{S,min}$ = –0.0421 au; $V_{S,max}$ = 0.1128 au), respectively. As the OH group in **2** is free to rotate around the C-O bond, the directionality of the HB sites on the OH may change, in principle making compound **2** more adaptable to the CSP chiral cavity than **1**. In the latter case, the rotation of the 4-pyridyl substituent does not change the directionality of the HB involving the pyridyl nitrogen.

Chiral columns based on C-3,5diMe, C-3Cl,4Me, C-4Cl,3Me, and C-3,5diCl were selected for this study in order to evaluate the impact of aryl chlorination on their enantioseparation performances. All columns contain selectors based on the same cellulose backbone which is derivatized with distinctive side chains determining the stereoelectronic properties of each selector [8]. The effect of introducing chlorine in the CSP structure is to modify the electron charge density distribution on the side chain moieties, thus the electron charge density on both C=O and phenyl ring decreases (π-acidity increases), whereas the acidity of the N–H increases [26]. This trend has been confirmed by calculating $V_{S,max}$ and $V_{S,min}$ values on pivotal regions of the side chains of C-3,5diMe, C-3Cl,4Me, C-4Cl,3Me, and C-3,5diCl (Table 1).

Table 1. Cellulose carbamate-based CSPs/columns used in the study, and $V_{S,max}$ and $V_{S,min}$ values associated with the main recognition sites (carbamate N–H and C=O)

Column[a)]	Ar (R',R''–C_6H_4)	Abbreviation	$V_{S,min}$ C=O (au)[b)]	$V_{S,max}$ N–H (au)[b)]
Cellulose-1	3,5-dimethyl	C-3,5diMe	–0.0630	0.0827
Cellulose-2	3-chloro-4-methyl	C-3Cl,4Me	–0.0576	0.0902
Cellulose-4	4-chloro-3-methyl	C-4Cl,3Me	–0.0578	0.0910

i-Cellulose-5	3,5-dichloro	C-3,5diCl	–0.0532	0.0987

[a] Lux series columns (Phenomenex Inc., Torrance, CA, USA). [b] V_S values calculated at DFT/B3LYP/6-311G* level, $V_{S,max}$ (Fig. 2C, maxima **a**) and $V_{S,min}$ (Fig. 2C, minima **b**)

It is known that the introduction of chlorine increases the fraction of free N–H groups [27], whereas the fraction of N–H involved in intramolecular HBs, contributing to maintain the high-ordered structure of the CSP, decreases. This could produce for the chlorinated CSPs a wider cavity available for the enantiomers with respect to the dimethylated selector, the overall enantioseparation resulting from the balance of carbamate polarity and intramolecular HB ability [27].

Chromatographic screening

The enantioseparability of TCIBPs **1** and **2** was tested on coated C-3,5diMe, C-3Cl,4Me, C-4Cl,3Me, and immobilized C-3,5diCl columns by using Hex/IPA 90:10 as MP. A comparison between the behaviours of the four columns is reported in Figure 3 (see Supporting Information, Table S2 for numerical data).

Good selectivity was achieved for the enantioseparation of **1** on C-3,5diMe (α = 2.82) exclusively, whereas lower selectivity values ranging from 1.07 to 1.15 were obtained in other cases. No enantioseparation was observed for **1** and **2** on C-3Cl,4Me and C-4Cl,3Me, respectively. Retention of both enantiomers was higher for **1** (average k_1 = 4.9; average k_2 = 6.4) compared to **2** (average k_1 = 2.1; average k_2 = 2.3) in almost all cases. The first eluted enantiomer of **2** showed higher retention only on C-3,5diMe (k_1 (**2**) = 2.94 vs k_2 (**1**) = 2.67). Given the presence of a HB acceptor (pyridyl nitrogen) as a distinctive recognition site, for compound **1** retention of the first eluted enantiomer tended to increase as the HB donor ability of the selector amidic N–H also increased (towards more positive $V_{S,max}$ values moving from C-3,5diMe to C-3,5diCl). The opposite trend was observed for compound **2** due to the presence of a HB donor (OH hydrogen) as distinctive recognition site. In this case, retention of both enantiomers increased as the N–H $V_{S,max}$ values and the electron charge density on the carbamate C=O decreased and increased (towards more negative $V_{S,min}$ values moving from C-3,5diCl to C-3,5diMe), respectively. As a particular case, retention of the second eluted enantiomer of compound **1** increased moving from C-3,5diMe (k_2 = 7.54) to C-3,5diCl (k_2 = 8.26), whereas the two chloromethyl substituted C-3Cl,4Me and C-4Cl,3Me provided lower k_2 values (4.78 and 5.15, respectively). On the other hand, EEO reversal was observed on C-3Cl,4Me and C-4Cl,3Me (*M-P*) for both compounds compared to the 3,5-disubstituted C-3,5diMe andcC-3,5diCl (*P-M*), this evidence revealing the occurrence of a different adsorption mechanism [3,28–31] It is worth noting that EEO is also a key factor for the method development [32]. Indeed, as chiral separation methods are optimized for optical purity control of a chiral analyte, the possibility to modify the EEO may be advantageous in order to have the minor enantiomer eluted first [28,31,32].

The addition of 5% MeOH to the MP was detrimental for retention and selectivity in almost all cases (Supporting Information, Table S3 and Fig. S3). However, for compound **1** on the C-3,5diMe the use of the mixture Hex/IPA/MeOH 90:5:5 contributed to reduce elution time (k_1, –12%; k_2, –52%) keeping selectivity value acceptable (α = 1.54) (Fig. S3A,B). In this regard, it is worth noting that the

addition of MeOH to the MP impacted retention of the second eluted enantiomer of compound **1** more on the C-3,5diMe (k_2, –52%) compared to the other chlorinated C-3Cl,4Me, C-4Cl,3Me, and C-3,5diCl (k_2, –17.6%, –32.6%, –34.4%, respectively). This suggested that a second key interaction involving the carbamate C=O possibly affected by 5% MeOH addition may participate in chiral recognition. In this regard, the involvement of a XB between the 2-iodine of compound **1** as XB donor and the carbonyl of the CSP as XB acceptor could be envisaged, the $V_{S,max}$ value on 2-iodine being higher for **1** (0.0535 au) compared to **2** (0.0496 au) [33].

This chromatographic results confirmed previous observations showing that the anisotropic properties of chiral substituted 4,4'-bipyridines strongly depend on the stereoelectronic features of the 2,2',3,3',5,5'-substituents bore by the orthogonal heteroaromatic rings, as a consequence of the atropisomeric motif [34,35]. For **1** and **2**, it was expected that the enantiodiscrimination degree should be related to the strength of noncovalent interactions involving both 2- and 2'- positions, due to the symmetry of the 3,3',5,5'-tetrachloro pattern. On the other hand, the direct contribution to retention and selectivity of the 4,4'-bipyridine core was shown to be low, in particular due to the weakness of the pyridine nitrogens as HB acceptors (–0.0490 au ≤ $V_{S,min}$ ≤ –0.0426 au). However, in compound **1** three electron-withdrawing heteroaromatic substructures polarized iodine, thus contributing to its capability to exert XB.

1.1.1 Effect of temperature on enantioseparation

With the aim to explore the impact of temperature on enantioseparation, and compare the thermodynamic profiles of the cellulose-based CSPs as derived from van 't Hoff analysis (see Supporting Information for details on van 't Hoff and thermodynamic equations), retention and selectivity of compounds **1** and **2** on the four cellulose-based CSPs were determined at different temperatures from 5 to 45°C in 5°C increments (Supporting Information, Tables S4–S7) using Hex/IPa 90:10 as MP. Several papers have dealt with theory of adsorption phenomena in chromatography, and with methods for profiling temperature dependence of retention and selectivity and thermodynamic quantities associated with the adsorption of analytes on the CSP surface [36,37]. Some studies stressed that thermodynamic quantities derived from the classical van 't Hoff equation are macroscopic entities which do not account for surface heterogeneity of the CSPs that determines individually achiral and chiral features of enantioseparation [38]. On the other hand, thermodynamic parameters depend on analyte, MP and the diffuse chiral (chirotopic) environment profile of the CSP. Therefore, the nature of the analyte/CSP contact can be explored on the basis of thermodynamic considerations, and useful information can emerge by comparison of thermodynamic data of analogue analyte/CSP pairs as subtle variations of the chromatographic system occur. In addition, temperature is a useful variable to optimize enantioseparation [3,39,40]. The thermodynamic quantities derived from van 't Hoff plots (Fig. 4) are reported in Table S8 (Supporting information). On this basis, the following remarks emerged:

i) compounds **1** and **2** showed different thermodynamic profiles, and the temperature dependence pattern was observed to be a function of the 2'-substituent structure and of the CSP type;

ii) for compounds **1** and **2** the enantioseparations were enthalpy-driven on the 3,5-disubstituted CSPs because the temperature range was below the calculated T_{ISO}, and the thermodynamic ratio $Q = \Delta\Delta H/(298 \times \Delta\Delta S) > 1$ [41] (157°C ≤ T_{ISO} ≤ 587°C; 1.44 ≤ Q ≤ 2.85) (Fig. 4A,B,G,H). On the contrary, the enantioseparations were shown to be entropy-driven on the 3,4-disubstituted CSPs in almost all cases (Fig. 4C,E,F) (–70°C ≤ T_{ISO} ≤ 15°C; 0.68 ≤ Q ≤ 0.97). These different thermodynamic profiles could explain the EEO reversal from *P-M* to *M-P* observed as the substitution pattern of the CSP phenyl rings changes from the 3,5- to 3,4-disubstitution;

iii) for compound **1** partial separation was observed on C-3Cl,4Me in the range 30–45°C (1.017 ≤ α ≤ 1.035) (Supporting Information, Fig. S4A), whereas for compound **2** on the C-4Cl,3Me very low enantioseparation was detectable at 45°C exclusively (α = 1.018) (Fig. S4B);

iv) in the case of compound **2** enantioseparation on C-3Cl,4Me, the thermodynamic profiles revealed the presence of two concurrent mechanisms in the range 5–45°C, an entropy controlled (T_{ISO} = –55°C, Q = 0.73) at low temperature and an enthalpy controlled mechanism (T_{ISO} = 97°C, Q = 1.24) at higher temperature. The two mechanisms coalesced between 30 and 20°C, providing at 25°C the best value of selectivity (α = 1.07), and a concave profile for the plot ln α = f(1/T) (Supporting Information, Fig. S5);

v) on this basis, enantioseparation of compounds **1** and **2** could in some cases be optimized by varying the temperature. For compound **1** on C-3,5diMe, elution time could be reduced at 45°C maintaining good selectivity ($\alpha_{25°C \rightarrow 45°C}$ = 2.83 → 2.32). In the other cases, enantioselectivity was almost independent of the temperature variation (Fig. S5). However, for **1** on C-4Cl,3Me, the enantioseparation under entropic control could be optimized at 45°C ($\alpha_{25°C \rightarrow 45°C}$ = 1.11 → 1.13). For both compounds **1** and **2** on C-3,5diCl, enantioseparation could be optimized under enthalpic conditions at 5°C ($\alpha_{25°C \rightarrow 5°C}$ (**1**) = 1.10 → 1.12; $\alpha_{25°C \rightarrow 5°C}$ (**2**) = 1.14 → 1.16).

Molecular dynamics simulations

As depicted in Figure 5, C-3,5diMe and A-3,5diMe [3] showed complementary enantioseparation ability towards compounds **1** and **2**. Indeed, compound **1** (Fig. 5A) (α = 2.82) was enantioseparated on the C-3,5diMe better than compound **2** (Fig. 5C) (α = 1.14), whereas **2** (Fig. 5D) (α = 1.26) was enantioseparated on the A-3,5diMe with selectivity higher than compound **1** (Fig. 5B) (α = 1.04). A backbone-dependent reversal of EEO was also observed, the elution sequence being *P-M* and *M-P* on C-3,5diMe and A-3,5diMe, respectively. In addition, thermodynamic analysis evidenced an enthalpic contribution to free energy difference (ΔΔG°) associated to the enantioseparations higher for C-3,5diMe (Q = 1.44, 1.60) compared to A-3,5diMe (Q = 1.04, 1.08). The enthalpic contribution to enantioseparation was higher for compound **2** compared to **1**, the difference being more pronounced on C-3,5-diMe ($\Delta Q_{1,2}$ = 0.16) compared to the amylose-based selector ($\Delta Q_{1,2}$ = 0.02).

On this basis, with the aim to explore the molecular basis of these chromatographic behaviors, a theoretical investigation based on MD simulations was performed by using C-3,5diMe and A-3,5diMe nonamers as virtual models of the polysaccharide-based selectors.

The 100 ns MD simulations in the AMBER force field [42] were performed by using the mixture Hex/IPA 90:10 as a virtual solvent in accord with the experimental conditions used in the chromatographic studies. With the aim to confirm the hypothesis that a XB involving the 2-iodine substituent of the enantiomer (*M*)-**1** could contribute to the high adsorption on C-3,5diMe (t_R = 30.25 min), the explicit σ-hole (ESH) concept [43,44] was used to model the electrophilic electron charge density depletion on the iodine atom [17] (see Supporting Information for details). For both analytes, the simulations were performed with and without ESH in order to also evaluate the MD results when the electrophilic character of iodine is suppressed. The total interaction energies calculated for (*M*)- and (*P*)-enantiomers of **1** and **2** in their complexes with each of the polysaccharide nonamer are summarized in Table 2.

Table 2. Binding energies (E_{int}) (kcal/mol) and component contributions (E_{el}, E_{vdW}) for the association of (*M*)-**1**, (*P*)-**1**, (*M*)-**2**, and (*P*)-**2** with C-3,5diMe (EEO_{exp} = *P*-*M*) and A-3,5diMe (EEO_{exp} = *M*-*P*)

	C-3,5diMe				A-3,5diMe			
TCIBP	**EEO_{calc}**	**E_{int}**	**E_{el}**	**E_{vdW}**	**EEO_{calc}**	**E_{int}**	**E_{el}**	**E_{vdW}**
1	*P*	–30.63	–3.43	–27.20	*M*	–32.16	–6.06	–26.10
	*M**	–33.23	–12.08	–21.15	*P*	–35.48	–6.03	–29.45
2	*P*	–31.76	–3.55	–28.21	*M*	–38.30	–9.49	–28.81
	M	–36.29	–13.78	–22.51	*P*	–41.25	–8.29	–32.96

* Explicit σ-hole was introduced on 2-iodine of (*M*)-**1**

The reported energies are mean values which were calculated from 5000 complexes obtained by snapshots taken every 20 ps from the 100 ns MD trajectories. The interaction energy (E_{int}) between enantiomer and selector is calculated on the basis of the energies of the selector-enantiomer complex, the selector and the enantiomer (eq. 1)

$$E_{int} = E_{total} - E_{enantiomer} - E_{polysaccharide\text{-}based\ selector} \quad (1)$$

where the E_{int} term derived from the contributions of the vdW and the electrostatic (el) interaction terms (eq. 2).

$$E_{int} = E_{el} + E_{vdW} \quad (2)$$

In Figure 6, representative snapshots and noncovalent interactions from the simulated MD trajectories of **1** and **2** complexes with C-3,5diMe (**A**-**D**) and A-3,5diMe (**E**-**H**) are depicted. The following remarks emerged:

i) in accord with previous observation [17], MD simulation provided a more compact structure for A-3,5diMe nonamer (with smaller cavities) compared to the C-3,5diMe;

ii) coherently, in all simulations involving the A-3,5diMe nonamers, the bulky iodine substituent protruded out of the polymer groove (Fig. 6F,G,H) or was oriented towards the void inside the groove (Fig. 6E), thus no XB was detected even if the ESH was introduced on the iodine. This finding is in accord with our previous observations on the detrimental effect of the compact structure of A-3,5diMe on XBs involving iodine [17];

iii) analogously, in all cellulose-based complexes involving the (*P*)-**1**, (*P*)-**2**, and (*M*)-**2** enantiomers, modelled either with and without ESH, the iodine was oriented outside the polymer (Fig. 6A,C,D);

iv) otherwise, a XB between the 2-iodine and the carbamate C=O was detected in the complex (*M*)-**1** / C-3,5diMe as the ESH was introduced on the iodine of the analyte. In this case, the calculated EEO (Table 2) is fully consistent with the experimental elution sequence. On the contrary, the simulation performed without ESH correction provided a theoretical EEO not consistent with experimental EEO, showing that the electrophilic feature of iodine has a pivotal role in the enantiodiscrimination. On this basis, the high retention of the enantiomer (*M*)-**1** was related to a four-component noncovalent interaction pattern consisting of one HB, two π-π interactions and a XB (Fig. 6B);

v) for each MD simulations, the E_{vdW} component was found to be the major contribution to the interaction energy. Indeed, in all cases, hydrophobic contacts between the haloaromatic scaffold of the analyte and the surface of the polymer appeared to govern analyte / selector association along with distinctive HBs and π- π stacking interactions;

vi) the fit of both enantiomers (*P*) on the C-3,5-diMe was very similar in accord with the close chromatographic retention values observed for the two *P*-enantiomers (t_R (**1**) = 13.00 min, t_R (**2**) = 14.00 min);

vii) in both **2** / A-3,5diMe complexes, each enantiomer is bound to the polysaccharide surface with the 4-hydroxyphenyl part protruding deeply inside the groove, and with the hydroxyl group engaged in HBs with carbamate sites, while buried into the hydrophobic environment generated by the nonpolar regions of the polymer. This profile is consistent with the high retention of both enantiomers of **2** on the A-3,5diMe (t_R (*M*) = 26.31 min, t_R (*P*) = 32.24 min) [3];

viii) finally, it is interesting to note that on the A-3,5diMe the 2'-(4-pyridyl) substituent was found in the external part of the surface (Fig. 6E;F), whereas the 2'-(4-hydroxyphenyl) substituent penetrated into the groove of the CSP, being blocked inside by HB interactions. Indeed, in this case, the hydroxyl group (and its associated recognition sites) is free to rotate around the C-O bond, protruding inside the chiral cavity as a molecular drill and making the analyte more adaptable compared to compound **1**.

Concluding remarks

The enantioseparation of TCIBPs **1** and **2** on 3,5-disubstituted (C-3,5diMe and C-3,5diCl) and 3,4-disubstituted (C-3Cl,4Me and C-4Cl,3Me) cellulose-based CSPs and related recognition mechanisms were explored through a multidisciplinary approach based on chromatographic and thermodynamic analysis, electrostatic potential analysis and MD simulations. Under NP elution conditions, lower selectivities were obtained in almost all cases compared to amylose-based selectors, which we had used in a previous study. The enantioseparation of 2'-(4-pyridyl)-TCIBP on C-3,5diMe represented an exception, and good selectivity could be obtained by using Hex/IPA 90:10 as MP (α = 2.82). Under these elution conditions, the analysis time was rather long (> 30 minutes). However, good selectivities could be obtained with shorter elution time by adding 5% MeOH to the MP (Hex/IPA/MeOH 90:5:5) (t < 20 min; α = 1.54) or by increasing elution temperature to 45°C (t < 22 min; α = 2.32).

EEO reversals dependent on the substitution pattern of the phenyl group of the CSPs were observed, the elution sequence being *P-M* and *M-P* on the 3,5- and 3,4-disubstituted CSPs, respectively, for both analytes. In particular, temperature-dependent enantioseparations performed in the range 5–45°C allowed for identifying enthalpy- ($T_{ISO} \geq 157$°C, $Q > 1$) and entropy-controlled ($T_{ISO} \leq 15$°C, $Q < 1$) profiles for 3,5- and 3,4-disubstituted CSPs, respectively.

The molecular bases of the complementary enantioseparation profiles and the backbone-dependent EEO reversal obtained for **1** and **2** on C-3,5diMe (*P-M*) and A-3,5diMe (*M-P*) were explored by MD simulations. Interaction energies calculated from 100 ns MD trajectories provided EEOs which were fully consistent with the experimental elution sequences. Analysis of calculated energies, analyte / selector complexes and noncovalent interaction patterns evidenced a) the more compact structure of the amylose-based polymer compared to the cellulose-based polysaccharide, and its capability to envelop the analytes which are able to penetrate into the cavity, b) the dominant contribution of van der Waals interactions to the overall analyte / selector binding, c) the pivotal role of the distinctive HB sites at the 2'-position of the TCIBP scaffold, inducing diverse adsorption mechanisms due to distinctive electronic and steric properties, d) the noncovalent interaction pattern causing the high adsorption of the enantiomer (*M*)-**1** on C-3,5diMe, and finally e) the contribution of a XB interaction to the adsorption of (*M*)-**1** on C-3,5diMe.

Acknowledgements

This work has been supported by Università Ca' Foscari Venezia, Italy (Dipartimento di Scienze Molecolari e Nanosistemi DSMN, ADIR funds).

The authors have declared no conflict of interest.

Data availability statement

The data that support the findings of this study are available in the supplementary material of this article.

References

[1] Scriba, G. K. E., *J. Chromatogr. A* 2016, 1467, 56–78.

[2] Lämmerhofer, M., *J. Chromatogr. A* 2010, *1217*, 814–856.

[3] Peluso, P., Sechi, B., Lai, G., Dessì, A., Dallocchio, R., Cossu, S., Aubert, E., Weiss, R., Pale, P., Mamane, V., Chankvetadze, B., *J. Chromatogr. A* 2020, *1625*, 461303.

[4] Peluso, P., Mamane, V., Dallocchio, R., Dessì, A., Cossu, S., *J. Chromatogr. A* 2020, *1623*, 461202.

[5] Peluso, P., Chankvetadze, B., *Anal. Chim. Acta* 2021, *1141*, 194–205.

[6] Hirschmann, H., Hanson, K. R., *Top. Stereochem.* 1983, *14*, 183–229.

[7] Mislow, K., Siegel, J., *J. Am. Chem. Soc.* 1984, *106*, 3319–3328.

[8] Chankvetadze, B., *TrAC Trends Anal. Chem.* 2020, *122*, 115709.

[9] Dessì, A., Peluso, P., Dallocchio, R., Weiss, R., Andreotti, G., Allocca, M., Aubert, E., Pale, P., Mamane, V., Cossu, S., *Molecules* 2020, *25*, 2213.

[10] Peluso, P., Dessì, A., Dallocchio, R., Mamane, V., Cossu, S., *Electrophoresis* 2019, *40*, 1881–1896.

[11] Koller, H., Rimböck, K.-E., Mannschreck, A. *J. Chromatogr. A* 1983, *282*, 89–94.

[12] Shao, Y., Molnar, L. F., Jung, Y., Kussmann, J., Ochsenfeld, C., Brown, S. T., Gilbert, A. T. B., Slipchenko, L. V., Levchenko, S. V., O'Neil, D. P., Di Stasio Jr., R. A., Lochan, R. C., Wang, T., Beran, G. J. O., Besley, N. A., Herbert, J. M., Lin, C. Y., VanVoorhis, T., Chien, S. H., Sodt, A., Steele, R. P., Rassolov, V. A., Maslen, P. E., Korambath, P. P., Adamson, R. D., Austin, B., Baker, J., Byrd, E. F. C., Dachsel, H., Doerksen, R. J., Dreuw, A., Dunietz, B. D., Dutoi, A. D., Furlani, T. R., Gwaltney, S. R., Heyden, A., Hirata, S., Hsu, C. -P., Kedziora, G., Khalliulin, R. Z., Klunzinger, P., Lee, A. M., Lee, M. S., Liang, W. Z., Lotan, I., Nair, N., Peters, B., Proynov, E. I., Pieniazek, P. A., Rhee, Y. M., Ritchie, J., Rosta, E., Sherrill, C. D., Simmonett, A. C., Subotnik, J. E., Woodcock III, H. L., Zhang, W., Bell, A. T., Chakraborty, A. K., Chipman, D. M., Keil, F. J., Warshel, A., Hehre, W. J., Schaefer, H. F., Kong, J., Krylov, A. I., Gill, P. M. W., Head-Gordon, M., *Phys. Chem. Chem. Phys.* 2006, *8*, 3172–3191.

[13] Frisch, M. J., Trucks, G. W., Schlegel, H. B., Scuseria, G. E., Robb, M. A., Cheeseman, J. R., Scalmani, G., Barone, V., Mennucci, B., Petersson, G. A., Nakatsuji, H., Caricato, M., Li, X., Hratchian, H. P., Izmaylov, A. F., Bloino, J., Zheng, G., Sonnenberg, J. L., Hada, M., Ehara, M., Toyota, K., Fukuda, R., Hasegawa, J., Ishida, M., Nakajima, T., Honda, Y., Kitao, O., Nakai, H., Vreven, T., Montgomery, J. A. Jr., Peralta, J. E., Ogliaro, F., Bearpark, M., Heyd, J. J., Brothers, E., Kudin, K. N., Staroverov, V. N., Keith, T., Kobayashi, R., Normand, J., Raghavachari, K., Rendell, A., Burant, J. C., Iyengar, S. S., Tomasi, J., Cossi, M., Rega, N., Millam, J. M., Klene, M., Knox, J. E., Cross, J. B., Bakken, V., Adamo, C., Jaramillo, J., Gomperts, R., Stratmann, R. E., Yazyev, O., Austin, A. J., Cammi, R., Pomelli, C., Ochterski, J. W., Martin, R. L., Morokuma, R. L., Zakrzewski, V. G., Voth, G., Salvador, P., Dannenberg, J. J., Dapprich, S., Daniels, A. D., Farkas, O., Foresman, J. B., Ortiz, J., Cioslowski, J., Fox, D. J., Gaussian 09, Revision B. 01; Gaussian. Inc.: Wallingford, CT, USA, 2010.

[14] Lu, T., Chen, F., *J. Comp. Chem.* 2012, *33*, 580–592.

[15] Lu, T., Chen, F., *J. Mol. Graph. Model.* 2012, *38*, 314–323.

[16] Case, D. A., Ben-Shalom, I. Y., Brozell, S. R., Cerutti, D. S., Cheatham, T. E. III, Cruzeiro, V. W. D., Darden, T. A., Duke, R. E., Ghoreishi, D., Gilson, M. K., Gohlke, H., Goetz, A. W., Greene, D., Harris, R., Homeyer, N., Huang, Y., Izadi, S., Kovalenko, A., Kurtzman, T., Lee, T. S., LeGrand, S., Li, P., Lin, C., Liu, J., Luchko, T., Luo, R., Mermelstein, D. J., Merz, K. M., Miao, Y., Monard, G., Nguyen, C., Nguyen, H., Omelyan, I., Onufriev, A., Pan, F., Qi, R., Roe, D. R., Roitberg, A., Sagui, C., Schott-Verdugo, S., Shen, J., Simmerling, C. L., Smith, J., Salomon-Ferrer, R., Swails, J., Walker, R. C., Wang, J., Wei, H., Wolf, R. M., Wu, X., Xiao, L., York, D. M., Kollman, P. A., AMBER 2018, University of California, San Francisco, 2018.

[17] Peluso, P., Mamane, V., Dallocchio, R., Dessì, A., Villano, R., Sanna, D., Aubert, E., Pale, P., Cossu, S., *J. Sep. Sci.* 2018, *41*, 1247–1256.

[18] Vogt, U., Zugenmaier, P., *Ber. Bunsenges. Phys. Chem* 1985, 89, 1217–1224.

[19] Yamamoto, C., Yashima, E., Okamoto, Y., *J. Am. Chem. Soc.* 2002, *124*, 12583–12589.

[20] Ye, Y. K., Bai, S., Vyas, S., Wirth, M. J., *J. Phys. Chem. B* 2007, *111*, 1189–1198.

[21] Martínez, J. M., Martínez, L., *J. Comput. Chem.* 2003, *24*, 819–825.

[22] Martínez, L., Andrade, R., Birgin, E. G., Martínez, J. M., *J. Comput. Chem.* 2009, *30*, 2157–2164.

[23] Pettersen, E. F., Goddard, T. D., Huang, C. C., Couch, G. S., Greenblatt, D. M., Meng, E. C., Ferrin, T. E., *J. Comput. Chem.* 2004, *25*, 1605–1612.

[24] Peluso, P., Cossu, S., *Chirality* 2013, *25*, 709–718.

[25] Yamada, Y., Ohyama, K., Onodera, G., Kuriyama, M., Kishikawa, N., Kuroda, N., *J. Chromatogr. A* 2015, *1425*, 173–179.

[26] Chankvetadze, B., *J. Chromatogr. A* 2012, *1269*, 26–51.

[27] Chankvetadze, B., Chankvetadze, L., Sidamonidze, S., Kasashima, E., Yashima, E., Okamoto, Y., *J. Chromatogr. A* 1997, *787*, 67–77.

[28] Matarashvili, I., Chankvetadze, L., Fanali, S., Farkas, T., Chankvetadze, B. *J. Sep. Sci.* 2013, *36*, 140–147.

[29] Vaňkátová, P., Kubíčková, A., Cigl, M., Kalíková, K. *J. Supercrit. Fluids* 2019, *146*, 217–225.

[30] Jakubec, P., Douša, M., Nováková, L. *J. Sep. Sci.* 2020, *43*, 2675–2689.

[31] Vaňkátová, P., Kubíčková, A., Kalíková, K., *Electrophoresis* 2021, *42*, 10.1002/elps.202000350.

[32] Tok, K. C., Gumustas, M., Jibuti, G., Suzen, H. S., Ozkan, S. A., Chankvetadze, B. *Molecules* 2020, *25*, 5865.

[33] Peluso, P., Mamane, V., Cossu, S., *Chirality* 2015, *27*, 667–684.

[34] Peluso, P., Mamane, V., Aubert, E., Cossu, S., *J. Chromatogr. A* 2014, *1345*, 182–192.

[35] Peluso, P., Mamane, V., Aubert, E., Cossu, S., *Electrophoresis* 2017, *38*, 1830–1850.

[36] Asnin, L. D., Stepanova, M. V., *J. Sep. Sci.* 2018, *41*, 1319–1337.

[37] Sepsey, A., Horváth, E., Catani, M., Felinger, A., *J. Chromatogr. A* 2020, *1611*, 460594.

[38] Fornstedt, T., *J. Chromatogr. A* 2010, *1217*, 792–812.

[39] Ianni, F., Pataj, Z., Gross, H., Sardella, R., Natalini, B., Lindner, W., Lämmerhofer, M., *J. Chromatogr. A* 2014, *1363*, 101–108.

[40] Matarashvili, I., Kobidze, G., Chelidze, A., Dolidze, G., Beridze, N., Jibuti, G., Farkas, T., Chankvetadze, B., *J. Chromatogr. A* 2019, *1599*, 172–179.

[41] Tanács, D., Orosz, T., Szakonyi, Z., Le, T. M., Fülöp, F., Lindner, W., Ilisz, I., Péter, A., *J. Chromatogr. A* 2020, *1621*, 461054.

[42] Maier, J. A., Martinez, C., Kasavajhala, K., Wickstrom, L., Hauser, K. E., Simmerling, C., *J. Chem. Theory Comput.* 2015, *11*, 3696–3713.

[43] Ibrahim, M. A. A., *J. Mol. Model.* 2012, *18*, 4625–4638.

[44] Kolar, M., Hobza, P., Bronowska, K., *Chem.Commun.* 2013, *49*, 981–983.

FIGURE CAPTIONS

Figure 1. Structures of chiral 4,4'-bipyridines **1** and **2** and cellulose-based chiral stationary phases.

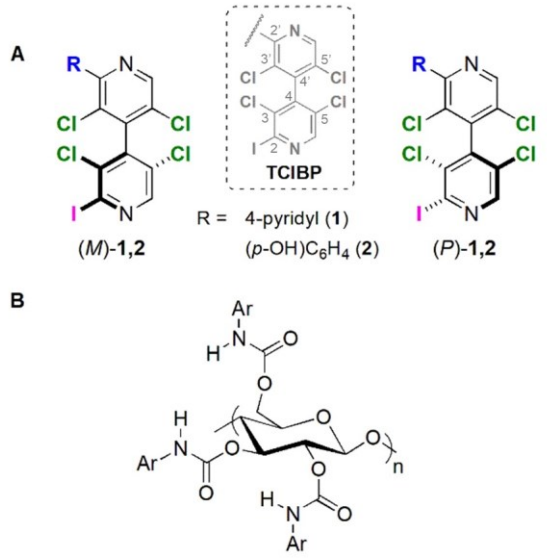

Figure 2. Maps of potential recognition sites of compounds **1** (**A**) and **2** (**B**), and of carbamate side chain of C-3,5diMe (**C**) described in terms of $V_{S,max}$ (pale blue) and $V_{S,min}$ (red) (values are reported in au) representation. For values associated to the *V* extrema **a** and **b** see Table 1.

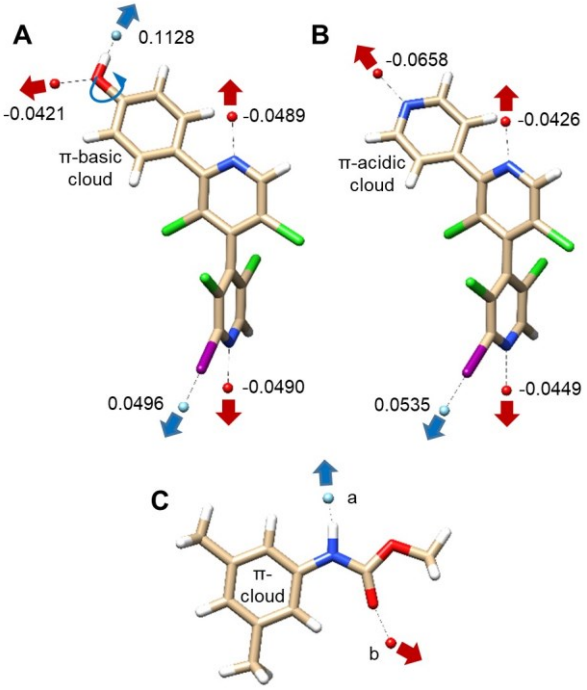

Figure 3. Correlation between retention range (*k* values) on four cellulose-based CSPs for compounds **1** and **2** and $V_{S,max}$ and $V_{S,min}$ values calculated on each cellulose carbamate recognition site (N–H and C=O).

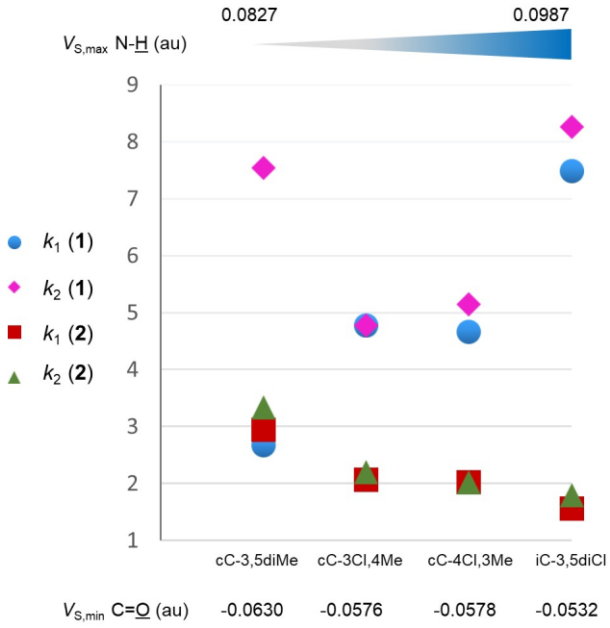

Figure 4. ln k_M and ln k_P vs 1/T plots for the enantioseparation of **1** and **2** on C-3,5diMe, C-3Cl,4Me, C-4Cl,3Me, and C-3,5diCl (Hex/IPA 90:10, *FR* = 0.8 ml/min, temperature range 278.15–318.15 K).

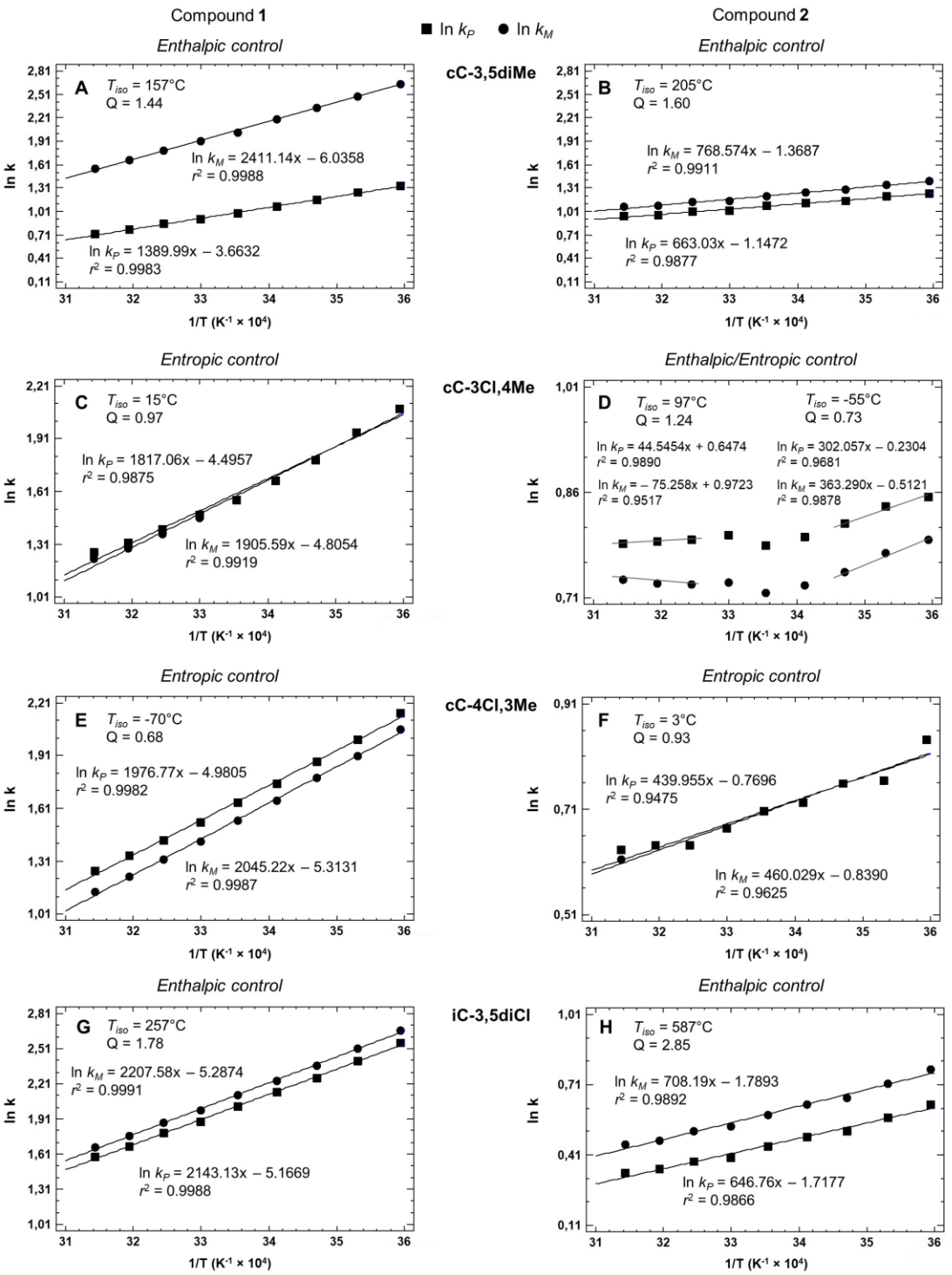

Figure 5. Chromatograms of enantioseparations of compounds **1** and **2** on C-3,5-diMe (**A** and **C**, respectively) and A-3,5-diMe (**B** and **D**, respectively) [3], MP = Hex/IPA 90:10, *FR* = 0.8 ml/min, T = 25°C.

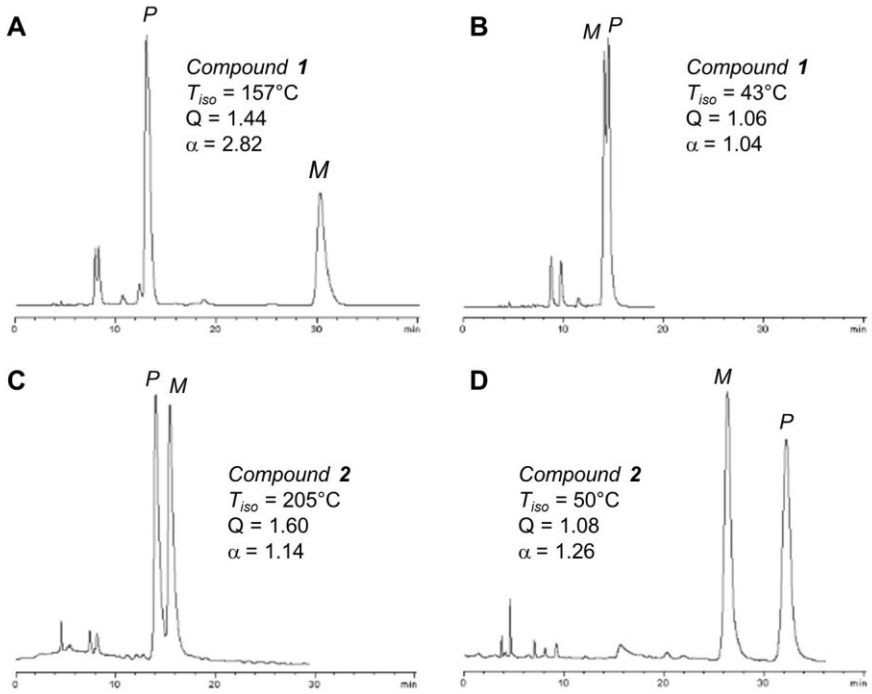

Figure 6. Representative snapshots and noncovalent interactions from the simulated MD trajectories of **1** and **2** complexes with C-3,5diMe (**A**-**D**) and A-3,5diMe (**E**-**H**).

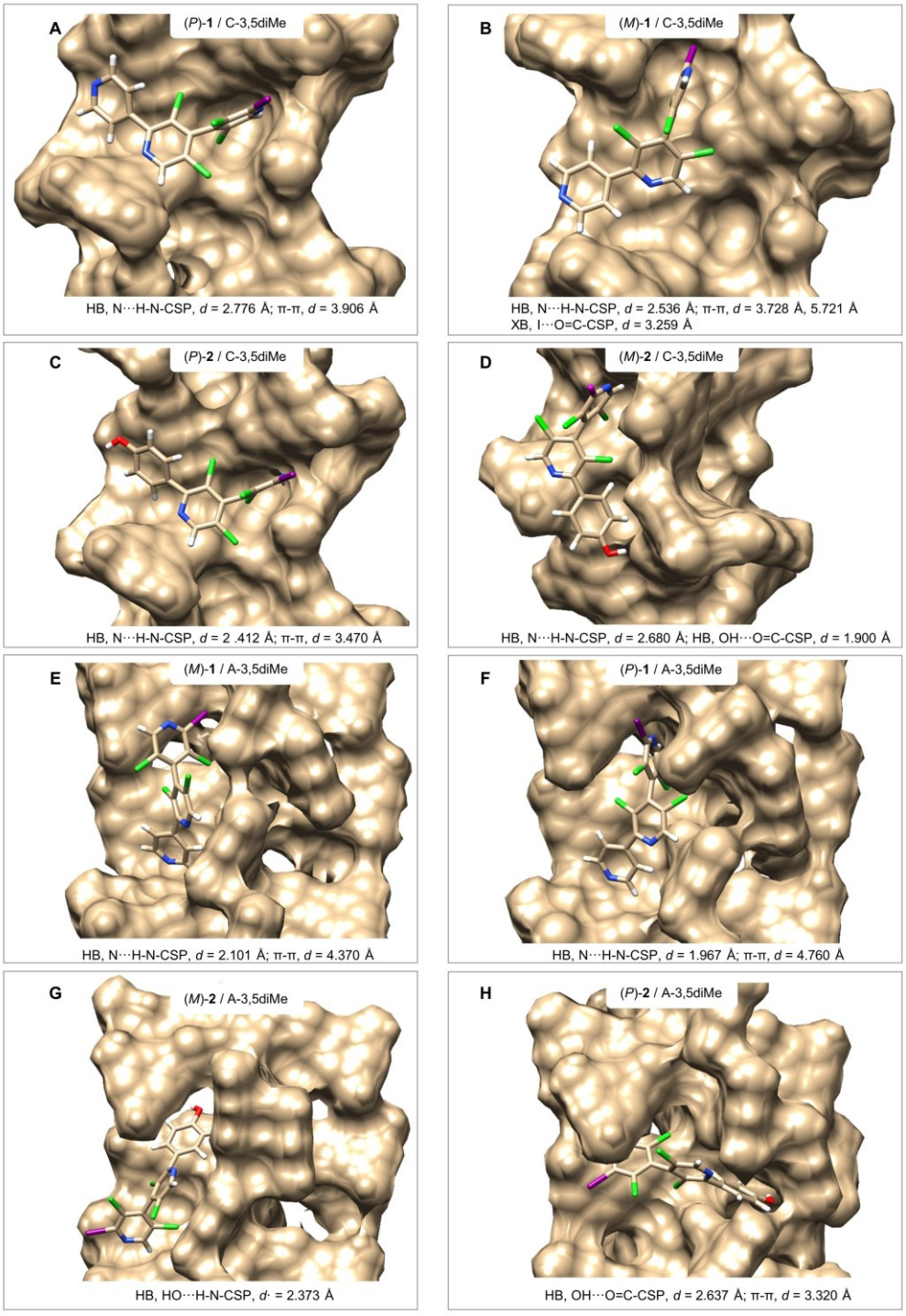

Supporting information

Supporting information file: Additional HPLC, thermodynamic and computational data.